NANO LETTERS

Letter

pubs.acs.org/NanoLett

Reusable, Robust, and Accurate Laser-Generated Photonic Nanosensor

Ali K. Yetisen,*[,†] Yunuen Montelongo,[‡] Fernando da Cruz Vasconcellos,[†] J.L. Martinez-Hurtado,[†] Sankalpa Neupane,[§] Haider Butt,[∥] Malik M. Qasim,[‡] Jeffrey Blyth,[†] Keith Burling,[⊥] J. Bryan Carmody,[#] Mark Evans,[§] Timothy D. Wilkinson,[‡] Lauro T. Kubota,[¶] Michael J. Monteiro,[□] and Christopher R. Lowe[†]

[†]Department of Chemical Engineering and Biotechnology, University of Cambridge, Tennis Court Road, Cambridge CB2 1QT, United Kingdom

[‡]Electrical Engineering Division, Department of Engineering, University of Cambridge, Cambridge CB3 0FA, United Kingdom

[§]Wellcome Trust/MRC Institute of Metabolic Science, University of Cambridge, Cambridge CB2 0QQ, United Kingdom

[∥]School of Mechanical Engineering, University of Birmingham, Edgbaston, Birmingham B15 2TT, United Kingdom

[⊥]Core Biochemical Assay Laboratory, Cambridge University Hospitals NHS Foundation Trust, Cambridge CB2 0QQ, United Kingdom

[#]Department of Pediatrics, Division of Nephrology, Eastern Virginia Medical School, Norfolk, Virginia 23507, United States

[¶]National Institute of Science and Technology of Bioanalytics, Institute of Chemistry, University of Campinas, Campinas, SP 13084-971, Brazil

[□]Australian Institute for Bioengineering and Nanotechnology, University of Queensland, Brisbane QLD 4072, Australia

Supporting Information

ABSTRACT: Developing noninvasive and accurate diagnostics that are easily manufactured, robust, and reusable will provide monitoring of high-risk individuals in any clinical or point-of-care environment. We have developed a clinically relevant optical glucose nanosensor that can be reused at least 400 times without a compromise in accuracy. The use of a single 6 ns laser (λ = 532 nm, 200 mJ) pulse rapidly produced off-axis Bragg diffraction gratings consisting of ordered silver nanoparticles embedded within a phenylboronic acid-functionalized hydrogel. This sensor exhibited reversible large wavelength shifts and diffracted the spectrum of narrow-band light over the wavelength range $\lambda_{peak} \approx 510-1100$ nm. The experimental sensitivity of the sensor permits diagnosis of glucosuria in the urine samples of diabetic patients with an improved performance compared to commercial high-throughput urinalysis devices. The sensor response was achieved within 5 min, reset to baseline in ~10 s. It is anticipated that this sensing platform will have implications for the development of reusable, equipment-free colorimetric point-of-care diagnostic devices for diabetes screening.

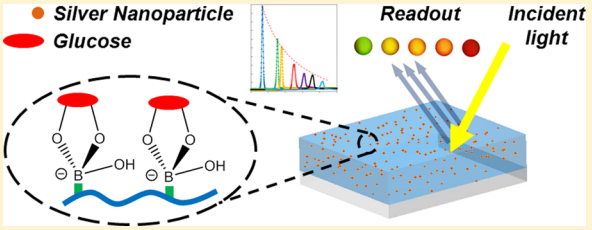

KEYWORDS: *Photonic sensors, glucose sensing, nanoparticles, diagnostics, point-of-care*

Glucose sensors comprising of optical transducers embedded into analyte-responsive materials are highly attractive for the development of healthcare monitoring systems.[1,2] The advantages of optical sensors over traditional dyes,[3] fluorescent molecules[4,5] and electrochemical[6−9] assays are that they (i) are not affected by electromagnetic fields, (ii) are label-free, (iii) enable sterile remote sensing, (iv) are amenable to miniaturization and multiplexing, and (v) are able to be used in real-time continuous monitoring.[10] Notable optical sensors have included photonic structures such as plasmonic nanomaterials,[11] hybrid gels,[12,13] crystal colloidal arrays,[14] and inverse opal hydrogels.[15] These analyte-responsive polymers have the added advantage of fine-tuning through a change in periodic structure, index of refraction, and/or localized surface plasmon resonance. Although these polymer optical sensors can be microfabricated, self-assembled, or a combination of both, there currently is no rapid and generic sensor fabrication technique capable of producing a narrow-band, uniform, reversible colorimetric readouts with a high-tunability range.

Here, we demonstrate an efficient strategy for the rapid fabrication of glucose-responsive reversible colorimetric photonic nanosensors. By combining the advantages of off-axis multibeam interference[16,17] and in situ size reduction of metallic nanoparticles[18] in boronic acid derivative function-

Received: April 3, 2014
Revised: May 5, 2014
Published: May 20, 2014

   dx.doi.org/10.1021/nl5012504 | Nano Lett. 2014, 14, 3587−3593

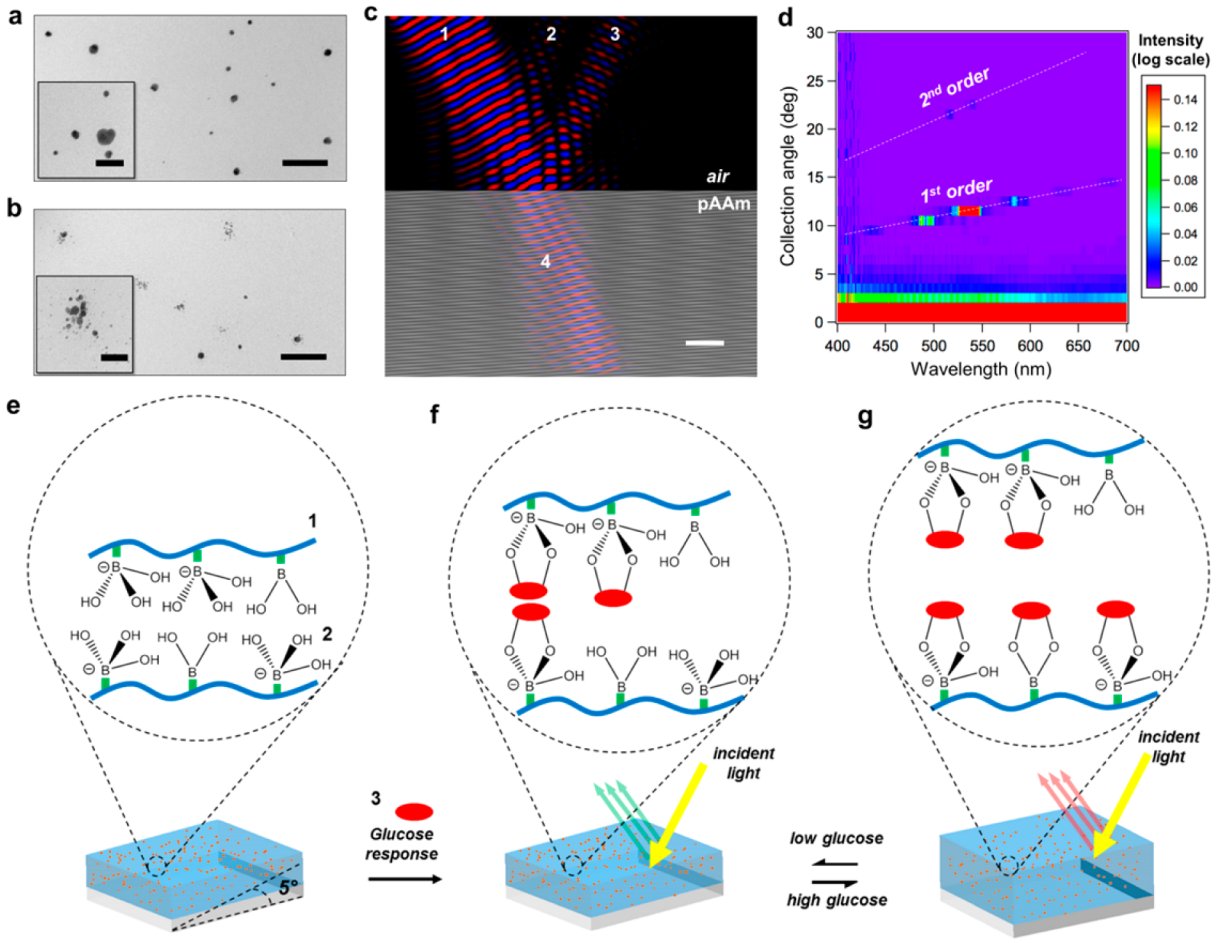

Figure 1. Optical characterization and principle of operation of the photonic nanosensor. TEM of the transverse section of pAAm matrix–Ag^0 NP system (a) before and (b) after exposure to the laser pulse showing reduction in the diameter of Ag^0 NPs at ablated planes. (c) A coherent source **1** of incident waves (λ = 532 nm) originating from air was propagated onto the sensor. The photonic structure reflects **3**, refracts **4**, and diffracts **2**, which allows offsetting the diffraction for reporting purposes. Scale bars: (a,b) = 200 nm, (c) = 2 μm, insets = 100 nm. Supporting Information Movie 1 demonstrates the interaction of the electromagnetic waves with the photonic structure. (d) Angular-resolved measurements of the diffracted light from the photonic structure. The intensity is on a logarithmic scale. (e) The sensor composed of pAAm-based hydrogel (**1**) functionalized with 3-APB (**2**) for sensing the target glucose (**3**). (f,g) Reversible swelling of the photonic nanosensor by glucose modulates both the Ag^0 NP distribution spacing and the refractive-index contrast, and systematically shifts the diffracted light from shorter to longer wavelengths as the hydrogel expands in the direction normal to the underlying substrate.

alized hydrogels[19] and implementing a new single-pulse laser writing technique, we produced visual colorimetric devices. Fully quantitative narrow-band (monochromatic) readouts were attained through spectrophotometry. The great advantages of our sensor over current technologies are (i) reusability, (ii) amenable to mass manufacturing through laser writing, (iii) readouts in visible as well as near-infrared regions of the spectrum, and (iv) reproducibility to sense glucose concentrations in the range of 0.1–375.0 mM with high analytical sensitivity using a low sample volume (<500 μL). Computational analysis allowed the optimization of this new glucose sensing platform, further allowing greater utility of the system in the response to other metabolites such as lactate and fructose. Clinical trials of the sensor in the urine samples of diabetic patients demonstrate that the sensor has significantly improved performance when compared with Multistix 10 SG read by CLINITEK Status + Analyzer (Siemens), while having comparable performance with fully automated Dimension Clinical Chemistry System (Siemens). Our glucose-responsive hydrogel-based colorimetric photonic nanosensor may have clinical applicability for diabetes screening or diagnosis of bacterial urinary tract infections.

Analysis of the nanoparticle size distribution, angular measurements, and determination of its pK_a value in combination with computational modeling of optical properties allowed optimization and utilization of the diffraction properties for sensing applications. Our nanosensor has a diffraction grating of Ag^0 nanoparticles (NPs) (ø ~ 15–25 nm) organized by the multibeam interference of a single 6 ns laser (λ = 532 nm, 200 mJ) pulse within a ~10 μm thick poly(acrylamide) (pAAm) matrix functionalized with 3-(acrylamido)-phenylboronic acid (3-APB). Supporting Information Figure S1 illustrates the step-by-step fabrication of the sensor through single-pulse laser writing. It was found that the Ag^0 nanoparticles after single-pulse laser photochemical patterning reduced in size as illustrated by the transmission electron microscopy (TEM) images of the transverse plane of the pAAm matrix–Ag^0 NP system in Figure 1a,b (see Supporting Information Figure S2). The magnified images of the nanoparticles in situ (see Insets) showed the reduction of size from ø = 32 ± 14 nm (n = 230) to ø = 16 ± 8 nm (n =

dx.doi.org/10.1021/nl5012504 | Nano Lett. 2014, 14, 3587–3593

429) before and after patterning. The changes in particle size, density, and periodicity of the Ag^0 NPs dictated the nanosensor's spectral response to the intensity and diffraction at different wavelengths.

Computational modeling allowed the evaluation of the optical characteristics of the pAAm matrix−Ag^0 NP system due to changes in particle size, density, and periodicity. Computing the interference originating from the superposition of three different waves, (1) the incident beam, (2) the beam reflected from the mirror, and (3) the beam reflected internally at the lower pAAm−water interface, produced a periodic structure along the pAAm gel's transverse section confined within a 20 × 10 μm^2 area (see Supporting Information Figure S3 for index of refraction measurements). Fresnel's law describes the paths of the incoming **1**, reflected **3**, and the refracted waves of light **4**. The diffracted wave **2** observed at 10° from the specular reflection (Figure 1c), obeyed Bragg's law, $n\lambda_{max} = 2d \sin(\theta)$, where n is an integer, and θ is the angle between incident ray and the surface of the photonic structure. The offset diffraction found from the device produced a narrow-band readout signal, allowing the differentiation of small changes in optical properties of the device due to different types and concentrations of analyte. The experimental spectral response of the sensor is shown in Figure 1d. At ∼10° from the specular reflection, the grating displayed narrow-band light at ∼530 nm, where the diffraction efficient was 2 orders of magnitude greater to the other wavelengths, confirming the existence of a periodic underlying photonic structure. These results correlate closely to that found by computational modeling, allowing these devices to be designed with predictive optical properties.

The measurement of urine glucose has diagnostic applicability in a variety of clinically relevant conditions.[20] Under normal conditions, the excretion rate of glucose in urine ranges between 0.30 and 1.70 mmol/24 h.[21] Because most filtered glucose is normally reabsorbed, an elevated urine glucose concentration indicates either impaired tubular reabsorption of glucose (e.g., familial renal glycosuria[22]), or more commonly, hyperglycemia that exceeds the kidney's reabsorptive capacity (e.g., diabetes mellitus[23]). Conversely, a low concentration of urine glucose may be found in urinary tract infections due to the bacterial metabolism of glucose.[24] Existing colorimetric and electrochemical tests are based on the glucose oxidase reaction.[25,26] However, their performance in detecting undiagnosed diabetes is limited due to low sensitivity (i.e., correctly identified patients with disease), which ranges from 21 to 64%.[27−30] False negative readings occur due to high detection limits and interference from medications (see Supporting Information Table S1).[31,32] While low-sensitivity tests may be useful,[33] false negatives can lead to a false sense of safety among users, and more critically delay correct diagnosis and early treatment.[30,34]

The fine changes in the lattice spacing through the matrix−analyte interaction provide a highly sensitive wavelength filter for glucose or other analyte sensing. To produce a glucose sensor, the pAAm hydrogel was functionalized with 3-APB (Figure 1e). Supporting Information Table S2 provides information about the composition of the glucose-responsive hydrogel. The reversible covalent bonds between 3-APB and the *cis*-diol units on glucose will change the hydrophilicity of the hydrogel and thus the periodic distribution of Ag^0 NPs. Boronic acid (pK_a = ∼8.8)[35,36] at low pH values is in an uncharged and trigonal planar configuration, and it can form the same complex to that found at high pH.[36] Supporting Information Figure S4 provides a description of this complexation mechanism. The binding of *cis*-diol groups results in the formation of boronate anions, which increases the system's Donnan osmotic pressure, and consequently swells the polymer hydrogel (Figure 1f,g).[2] Swelling produces an increase in the distance of the periodically organized Ag^0 NP regions and shifts the diffracted light peak to longer wavelengths.

Our nanosensor's response to an increase in clinically relevant concentrations of glucose (1.0 to 10.0 mM) in artificial urine showed a shift of the diffracted light from shorter to longer wavelengths under physiological conditions (pH 7.40). Supporting Information Table S3 shows the composition of the artificial urine. Figure 2a illustrates a typical narrow-band spectral readout at pH 7.40, indicating a decrease in the diffraction efficiency and peak broadening exhibited by the photonic structure as the concentration of glucose increased. This optical effect can be attributed to the decrease in the density of Ag^0 NPs present in the periodic regions as the polymer matrix expands in the direction normal to the underlying substrate. This expansion reduces the effective index contrast between these regions and the medium, thus resulting in a decrease of the absorbance strength of the localized surface plasmon resonance. We also infer that the trend is asymptotical due to an inverse correlation between the concentration of Ag^0 NPs in the system and the lattice spacing (d) of the density concentrated regions (layers). Hence, the maximum peak intensity (I_{max}) and its corresponding wavelength λ_{max} is inversely related to the periodicity of the layers because of the reduction in the contrast of the effective refractive index during lattice expansion. This relation can be expressed as $I_{max} = c/\lambda_{max}$, where c is a constant, assuming that asymptotes approach zero. However, in our pAAm matrix−Ag^0 NP system, where the polymer expansion is finite and the asymptotes do not approach zero, the maximum intensity (I_{max}) at a given λ_{max} can be expressed as

$$I_{max} \approx I_0 + \frac{c}{\lambda_{max} - \lambda_0} \quad (1)$$

where I_0 and λ_0 represent the asymptotes of the curve. Additionally, the displacement of the asymptotes regarding the first order can be attributed to other factors such as the scattering strength of each Ag^0 NP, which increases at Mie plasmon resonances in the blue/green region, hence the total amount of scattering decreases as the Bragg resonance shifts to longer wavelengths. The spectrophotometer used in the diffraction measurements had a wavelength shift resolution of 0.50 nm, which corresponds to a minimum lattice swelling distance of ∼0.17 nm calculated from Bragg's law. The ∼10 μm thick hydrogel matrix can theoretically accommodate ∼55 Ag^0 nanoparticle-based fringes. Therefore, a minimum of ∼9.40 nm of total hydrogel swelling normal to the underlying substrate is required to cause a resolvable spectral shift.

The wavelength of the diffraction peak was ∼565 nm for glucose-free artificial urine, and additions of up to 10.0 mM glucose shifted this peak systematically by 21, 81, 356, 379, and 420 nm at pH values of 7.00, 7.25, 7.40, 7.75, and 8.00 (Figure 2b); resulting in the limit of detection of 0.61, 0.50, 0.41, 0.36, 0.26 mM, respectively. The diffraction exhibited green, yellow, orange, and red light before moving into the near-infrared region with further increases in glucose concentration (inset in Figure 2b). Figure 2c illustrates that based on the Henderson−Hasselbalch equation, the apparent pK_a value of the nanosensor was ∼8.5, while the sensor displayed improved sensitivity as the

dx.doi.org/10.1021/nl5012504 | Nano Lett. 2014, 14, 3587−3593

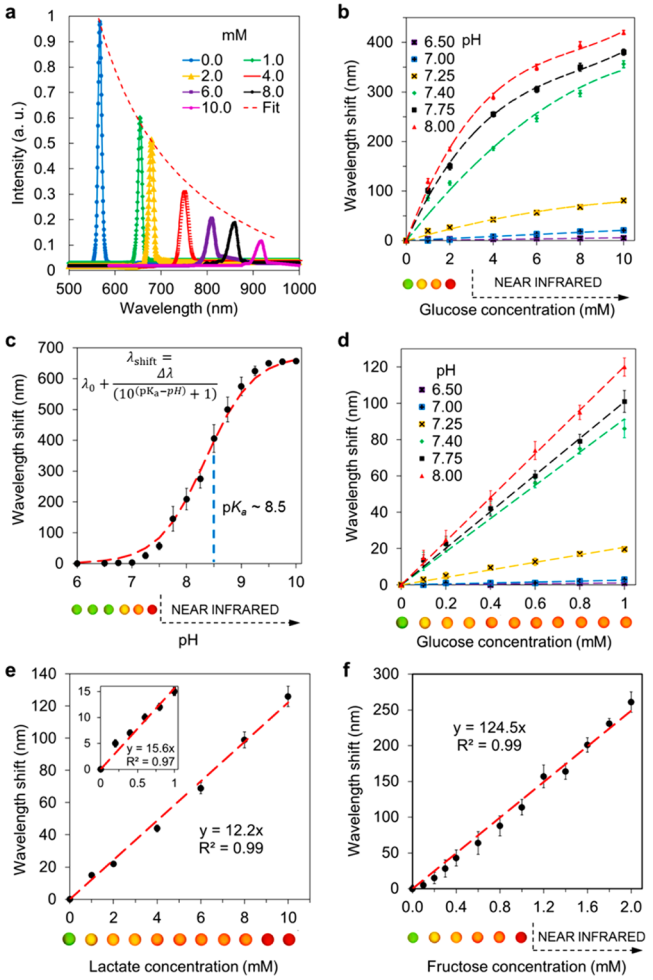

Figure 2. Response of the photonic nanosensor to glucose, lactate, and fructose. (a) An increase in the glucose concentration of artificial urine solutions (pH 7.40) swelled the polymer matrix, thus causing a shift in the diffracted light peak to longer wavelengths, while also showing a correlation between the intensity and the wavelength observed (n = 7). Constants for the fit: c = 260 nm, λ_0 = 366 nm, I_0 = −0.32, and a.u. = arbitrary units. (b) Spectral readout at pH values from 6.50 to 8.00 (n = 126). The inset shows the colorimetric response at pH 7.40. (c) Determination of apparent pK_a of the pAAm matrix−Ag^0 NP system. The apparent pK_a value for the 3-APB functionalized pAAm matrix was calculated using the Henderson−Hasselbalch equation, where $\lambda_{shift,0-16}$ = step wavelength shift, λ_0 = initial wavelength and $\Delta\lambda$ = ($\lambda_{max\ final} - \lambda_0$) overall wavelength difference (n = 48). The inset shows colorimetric readouts of the sensor as a function of pH. (d) The wavelength shift as a function of glucose concentration (<1.0 mM) shows reproducibility (±~5 nm) over three trials (n = 126). The inset shows the colorimetric response at pH 7.40. (e) An increase in the concentration (10.0 mM) of lactate in artificial urine (pH 7.40) swells the polymer matrix, causing a shift in the diffraction wavelength from ~563 to ~689 nm; lower lactate concentrations (0.1−10.0 mM) caused a shift from ~563 to ~578 nm (see upper inset) (n = 39). The lower inset shows the colorimetric readouts. (f) Diffraction wavelength shift of the photonic nanosensor in response to an increase in concentrations of fructose in artificial urine. An increase in the concentration (2.0 mM) of fructose in artificial urine expands the polymer matrix, thus causing a shift in diffraction wavelength from ~565 to ~825 nm (n = 39). The inset shows the colorimetric readouts. Standard error bars represent three independent samples.

pH was increased from 6.0 to 10.0 (see inset for the colorimetric readouts). Therefore, with this pK_a we would expect the glucose to bind to the tetrahedral form with degrees of ionization of 0.4, 3.2, 4.9, 17.8 and 25.7% at pH values of 7.00, 7.25, 7.40, 7.75, and 8.00, and subsequently reach equilibrium. At low concentrations, glucose binds with the boronic acid groups in a tetrahedral coordination form[2] in which the binding transforms, although kinetically slower, to a trigonal planar form at higher concentrations. A decrease in the slope was consequently observed at the higher concentration range.

The potential clinical utility of our highly sensitive sensor in detecting hypoglycosuria associated with urinary tract infections was tested by quantifying glucose concentrations below 1.0 mM. When bacteria are present in urine, they metabolize existing glucose, decreasing its concentration below 1.0 mM.[37] Therefore, measuring low concentrations of urine glucose with high sensitivity can be used for rapid screening of urinary tract infections,[24] and through the detection and early treatment urinary tract infections may reduce the risk of chronic kidney failure due to renal scarring.[38,39] We show in Figure 2d quantification of the glucose concentration from 0.1 to 1.0 mM in artificial urine solutions by the systematic shift of the diffraction peak to longer wavelengths (see Supporting Information Figure S5 for spectral readouts and inset in Figure 2d for colorimetric response). A wavelength shift from 3 to 120 nm with a systematic increase in pH from 7.00 to 8.00 gave concentration detection limits ranging from 240 to 90 μM, respectively.

The *cis*-diol groups of 3-APB can competitively bind to lactate and fructose along with glucose. Although lactate is present at low concentrations in urine (0.01−0.25 mmol/L,[40] which may increase during physical activity), it can competitively bind through its α-hydroxy acid with boronic acid bound groups in the hydrogel. While at high concentrations (10.0 mM) of lactate, a shift of ~125 nm was measured (Figure 2e), at low concentrations (<1.0 mM) of lactate a wavelength shift of ~15 nm was measured (upper inset in Figure 2e) (see Supporting Information Figure S6 for the spectral readouts and lower inset in Figure 2e for colorimetric response). At normal lactate concentrations in urine of ~1.0 mM,[21] the corresponding interference of lactate resulted in a wavelength shift of up to 15 nm. The measurement error due to lactate interference for the diagnosis of glucosuria (10.0 mM) and urinary tract infections (<1.0 mM) was ~4.2 and ~13.6%, respectively. In addition to lactate, we evaluated competitive binding to fructose. Normal fructose excretion in urine is 37.7 ± 23.0 μmol/day.[41] The concentration of fructose in urine may be elevated due to excessive dietary sugar intake. Both natural and added sugar contain significant amounts of fructose,[42] and dietary sugar consumption is proportional to the urinary excreted fructose[43] because a fraction of ingested fructose escapes hepatic metabolism and passes into the systematic circulation, where it is excreted in the urine.[44] To assess its interference, we tested our nanosensor with different concentrations of fructose in artificial urine. We measured wavelength shifts of ~115 and ~260 nm in the presence of 1.0 and 2.0 mM of fructose, respectively (Figure 2f) (see Supporting Information Figure S7 for the spectral readouts). Inset in Figure 2f shows the colorimetric response. In addition to fructose and lactate, we also investigated variation in osmolality (see Supporting Information Figure S8).

The sensor's response was reproducible within ±5 nm over successive (consecutive swelling/shrinking steps) artificial urine changes after equilibrium was reached (<3 nm) at 24 °C, and

dx.doi.org/10.1021/nl5012504 | Nano Lett. 2014, 14, 3587−3593

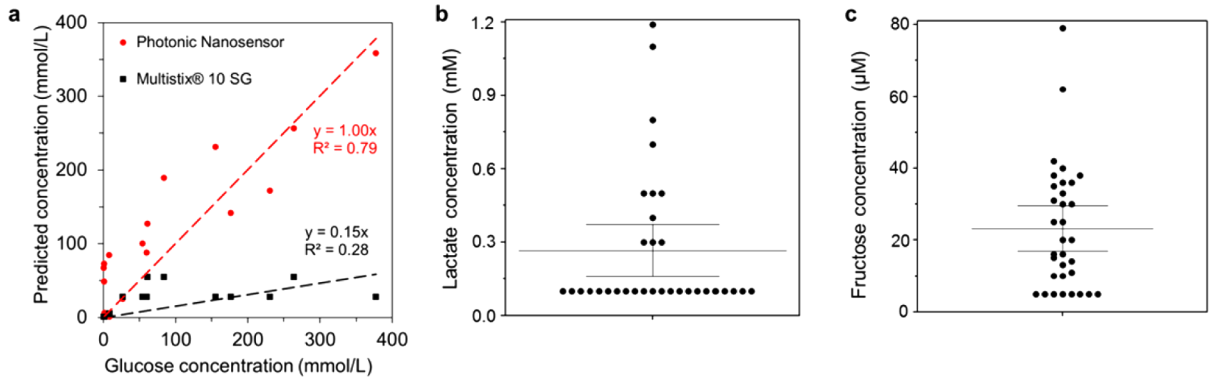

Figure 3. Performance of the photonic nanosensor in urine testing and control experiments. (a) Photonic nanosensor and its performance comparison with Multistix 10 SG read by CLINITEK Status + Analyzer, and Dimension Clinical Chemistry System. (b) Measurements of lactate concentrations. (c) Measurements of fructose concentrations. Middle horizontal lines in (b) and (c) represent the mean. Data points represent individual urine specimens (n = 33). Error bars represent upper and lower 95% confidence intervals of the mean.

no hysteresis was detected during these trials. At low concentrations of glucose (<1.0 mM), the sensor required ~50 min to reach ~90% equilibrium. However, at high glucose concentrations (>1.0 mM), the sensor exhibited a response time of ~1.5 h to reach ~90% equilibrium. The sensor's response to fructose showed a comparable turnaround time, but the sensor responded significantly faster to lactate, reaching ~90% equilibrium in 3 min for a 10.0 mM solution. For lactate concentrations of <1.0 mM, the sensor reached 90% equilibrium under ~20 s.

We also tested anonymized urine samples collected from patients with diabetes attending the Wolfson Diabetes and Endocrine Clinic (Addenbrooke's Hospital, U.K.) in February 2014. The composition of the photonic sensor was optimized to allow for testing samples with up to 375 mM concentrations of glucose. Supporting Information Figure S9 illustrates the calibration of the optimized sensor. The reliability of the glucose sensor was evaluated by quantifying the glucose concentration in urine samples of diabetic patients (n = 33). In order to decrease the turnaround time in analysis, the rate of wavelength shift was correlated with the concentration of glucose in the sample. By analyzing this dynamic shift, we predicted the characteristics of the nanosensor at a given glucose concentration. The novelty of this approach is that an accurate estimation of glucose concentration can be achieved without waiting for equilibrium. In testing of urine samples, the peak wavelength at the maximum intensity was measured from 1 to 5 min with 1 min increments. The sensor was reset in ~10 s and it was ready to use for the next measurement immediately. When we observe the wavelength shift in time (0–5 min), the rate of wavelength shift decreases as the time increases based on the decrease of boronic acid groups in tetrahedral coordination form. As the time lapses, the binding mechanism transforms to trigonal planar form, which is kinetically slower. Therefore, the rate of change of bound molecules $n(t)$ is proportional to the total number of glucose N_g molecules and the total number of boronic acid groups N_f:

$$\frac{dn(t)}{dt} \propto (N_g - n(t))(N_f - n(t)) = a(N_g - n(t))(N_f - n(t)) \quad (2)$$

When the wavelength shift is proportional to the amount of binding of *cis*-diol groups to glucose molecules, this expression can be expressed as

$$\frac{d\lambda(t)}{dt} \propto (C_g - \Delta\lambda(t))(C_f - \Delta\lambda(t)) = a(C_g - \Delta\lambda(t))(C_f - \Delta\lambda(t)) \quad (3)$$

where C_g and C_f are constants with proportionality to *cis*-diol and glucose molecules present. The solution of this equation is nontrivial to be fit with the experimental data; instead the numerical solution of $d\lambda(t)/dt$ has been obtained from the data. Thus, two values were plotted, and a quadratic solution was fit to the equation to obtain the variables C_g and C_f. As the solution was commutable, the minimum value was considered as C_g. A linear fitting was applied to these values and correlated to the concentration of glucose found with Multistix 10 SG strips read by CLINITEK Status + Analyzer and fully automated Dimension Clinical Chemistry System (Figure 3a). The results show a good agreement between the photonic nanosensor and Dimension Clinical Chemistry System, while no false negatives were observed. As can be seen from Figure 3a, the photonic nanosensor had an improved correlation coefficient (R^2) of 0.79 when compared with Multistix 10 SG (0.28). It was also noted that the Multistix 10 SG reported results significantly lower than Dimension Clinical Chemistry System and photonic nanosensor. Figure 3b illustrates scatter dot plot of measured lactate concentration values (μ = 0.27 mM, 95% CI_{low} = 0.16 mM, 95% CI_{high} = 0.37 mM) (see Supporting Information Figure S10 for each data point), while Figure 3c shows measured fructose concentration values (μ = 23.18 μM, 95% CI_{low} = 16.93 μM, 95% CI_{high} = 29.43 μM) (see Supporting Information Figure S11 for each data point).

We demonstrated a photonic nanosensor with potential point-of-care clinical applicability for diabetes screening or diagnosis of urinary tract infection. Our nanosensor was fabricated in an ultrafast approach by using a single 6 ns laser pulse to produce diffraction gratings consisting of periodic Ag^0 NP distribution regions that are separated ~ $\lambda/2$ apart in a glucose-sensitive pAAm matrix. Overall, the sensor displayed large wavelength shifts while also being suitable for multiple analyses. We measured the response of the sensor due to variation in physiological glucose concentrations in the range of 0.1 to 375.0 mM with a detection limit of 90 μM. We have shown that when the boronic acid moieties bind to the *cis*-diol groups of glucose, the diffraction peak of the sensor shifted to longer wavelengths, producing a visual change in color. In addition, we further tested the response to the presence of

dx.doi.org/10.1021/nl5012504 | Nano Lett. 2014, 14, 3587–3593

lactate and fructose. For the determination of glucosuria (>10.0 mM of glucose), while the interference from normal urinary lactate represented 1.57% of the signal, interference from normal urinary fructose[41] was 0.32%. For monitoring of urinary tract infections (<1.0 mM of glucose), the interference from normal urinary lactate and fructose were 6.21 and 1.33%, respectively (see Supporting Information Table S4 for selectivity assessment). The readouts were achieved within 5 min with the reset time of ∼10 s. In the diagnosis of glucosuria in urine samples, the photonic nanosensor showed improved performance compared to commercial glucose test strips, while showing comparable performance with fully automated analyzers. The range of spectral readouts can be finely controlled by changing the wavelength of the laser light and the chemistry of the exposure bath (Supporting Information Figure S12); the sensitivity of the photonic sensor can be modulated by varying the concentration of the cross-linker and the functional groups in the polymer matrix (Supporting Information Figure S13). In the realization of our nanosensor, the pH of urine can be corrected using analytical methods, while the osmolality can be standardized using glucose/creatinine ratio. While the present study focused on urinalysis as a noninvasive test, further investigations may involve optimization of the photonic nanosensors for use in blood. Moving forward, practical approaches may require a microfluidic, lab-on-a-chip multiplexed assay, which could be read by a smartphone application[45] to achieve a commercial device.

Our photonic sensing platform has flexibility in controlling the angle of off-axis diffraction precisely as well as the diffraction pattern while offering a narrow-band response for semiquantitative visual colorimetric readouts and fully quantitative readouts. Ultrafast nanosecond laser writing of photonic nanosensors has the potential for producing equipment-free and scalable analytical devices. The technology is applicable to in vitro diagnostics as well as implantable in vivo sensors because it can operate in both visible and infrared regions. We envision that rapidly fabricating photonic nanosensors will enable the development of colorimetric tests for monitoring metabolic disorders and infectious diseases at clinical settings and point-of-care.

■ ASSOCIATED CONTENT

Supporting Information

A movie showing propagation of the electromagnetic waves from air onto the photonic nanosensor, list of medications and other agents that interfere with the glucose-oxidase reaction, methods, preparation of the glucose-responsive hydrogels, preparation of the photographic developer, nanoparticle formation in the polymer matrix, photochemical laser patterning of nanosensors, TEM analysis, index of refraction measurements, computational modeling, complexation of boronic acid derivatives with glucose, spectral analysis of the nanosensors, preparation of artificial urine samples, determination of the apparent pK_a, preparation of urine samples, selectivity assessment, colorimetric glucose tests, colorimetric lactic acid tests, fructose assay, materials, equipment, and laser safety. This material is available free of charge via the Internet at http://pubs.acs.org.

■ AUTHOR INFORMATION

Corresponding Author

*E-mail: ay283@cam.ac.uk.

Author Contributions

A.K.Y., F.C.V., and C.R.L. designed the project. A.K.Y. and F.C.V. prepared the sensors. A.K.Y. and Y.M. performed the optical characterization and analysis. A.K.Y, S.N., and K.B. performed the clinical trials. A.K.Y., Y.M., F.C.V., J.L.M.H., H.B., M.M.Q., J.B., J.B.C., M.E., T.D.W., L.T.K., M.J.M., and C.R.L. wrote the manuscript.

Notes

The authors declare no competing financial interest.

■ ACKNOWLEDGMENTS

Assays were performed by the NIHR Cambridge Biomedical Research Centre, Core Biochemical Assay Laboratory. We thank Jakub Tomasik for discussions. We acknowledge FAPESP (Grant 2011/06906-6) and CNPq INCTBio (Grant 209869/2013-5).

■ REFERENCES

(1) Wu, Q.; Wang, L.; Yu, H.; Wang, J.; Chen, Z. *Chem. Rev.* **2011**, *111*, 7855−7875.
(2) Guan, Y.; Zhang, Y. *Chem. Soc. Rev.* **2013**, *42*, 8106−21.
(3) Bankar, S. B.; Bule, M. V.; Singhal, R. S.; Ananthanarayan, L. *Biotechnol. Adv.* **2009**, *27*, 489−501.
(4) Cummins, B. M.; Garza, J. T.; Cote, G. L. *Anal. Chem.* **2013**, *85*, 5397−404.
(5) Liu, Y.; Deng, C.; Tang, L.; Qin, A.; Hu, R.; Sun, J. Z.; Tang, B. Z. *J. Am. Chem. Soc.* **2011**, *133*, 660−3.
(6) Zhai, D.; Liu, B.; Shi, Y.; Pan, L.; Wang, Y.; Li, W.; Zhang, R.; Yu, G. *ACS Nano* **2013**, *7*, 3540−6.
(7) Invernale, M. A.; Tang, B. C.; York, R. L.; Le, L.; Hou, D. Y.; Anderson, D. G. *Adv. Healthcare Mater.* **2014**, *3*, 338−42.
(8) Guo, C.; Huo, H.; Han, X.; Xu, C.; Li, H. *Anal. Chem.* **2014**, *86*, 876−83.
(9) Wooten, M.; Karra, S.; Zhang, M.; Gorski, W. *Anal. Chem.* **2014**, *86*, 752−7.
(10) Steiner, M. S.; Duerkop, A.; Wolfbeis, O. S. *Chem. Soc. Rev.* **2011**, *40*, 4805−39.
(11) He, H.; Xu, X.; Wu, H.; Jin, Y. *Adv. Mater.* **2012**, *24*, 1736−40.
(12) Wu, W.; Mitra, N.; Yan, E. C.; Zhou, S. *ACS Nano* **2010**, *4*, 4831−9.
(13) Wu, W. T.; Shen, J.; Li, Y. X.; Zhu, H. B.; Banerjee, P.; Zhou, S. Q. *Biomaterials* **2012**, *33*, 7115−7125.
(14) Muscatello, M. M.; Stunja, L. E.; Asher, S. A. *Anal. Chem.* **2009**, *81*, 4978−86.
(15) Honda, M.; Kataoka, K.; Seki, T.; Takeoka, Y. *Langmuir* **2009**, *25*, 8349−56.
(16) Fuchs, Y.; Kunath, S.; Soppera, O.; Haupt, K.; Mayes, A. G. *Adv. Funct. Mater.* **2014**, *24*, 688−694.
(17) Naydenova, I.; Jallapuram, R.; Toal, V.; Martin, S. *Appl. Phys. Lett.* **2008**, *92*, 031109−1−3.
(18) Yetisen, A. K.; Butt, H.; da Cruz Vasconcellos, F.; Montelongo, Y.; Davidson, C. A. B.; Blyth, J.; Chan, L.; Carmody, J. B.; Vignolini, S.; Steiner, U.; Baumberg, J. J.; Wilkinson, T. D.; Lowe, C. R. *Adv. Opt. Mater.* **2014**, *2*, 250−254.
(19) Zhang, C. J.; Losego, M. D.; Braun, P. V. *Chem. Mater.* **2013**, *25*, 3239−3250.
(20) Simerville, J. A.; Maxted, W. C.; Pahira, J. J. *Am. Fam. Physician* **2005**, *71*, 1153−62.
(21) Kratz, A.; Ferraro, M.; Sluss, P. M.; Lewandrowski, K. B. *N. Engl. J. Med.* **2004**, *351*, 1548−63.
(22) Scholl-Burgi, S.; Santer, R.; Ehrich, J. H. H. *Nephrol., Dial., Transplant.* **2004**, *19*, 2394−2396.
(23) Ferrannini, E. *Diabetes* **2011**, *60*, 695−6.
(24) Scherstén, B.; Dahlqvist, A.; Fritz, H.; Köhler, L.; Westlund, L. *JAMA, J. Am. Med. Assoc.* **1968**, *204*, 205−208.
(25) Wang, J. *Chem. Rev.* **2008**, *108*, 814−25.
(26) Heller, A.; Feldman, B. *Chem. Rev.* **2008**, *108*, 2482−2505.

(27) Davies, M. J.; Williams, D. R.; Metcalfe, J.; Day, J. L. *Q. J. Med.* **1993**, *86*, 677−84.
(28) Engelgau, M. M.; Narayan, K. M.; Herman, W. H. *Diabetes care* **2000**, *23*, 1563−80.
(29) Hanson, R. L.; Nelson, R. G.; McCance, D. R.; Beart, J. A.; Charles, M. A.; Pettitt, D. J.; Knowler, W. C. *Arch. Int. Med.* **1993**, *153*, 2133−40.
(30) Friderichsen, B.; Maunsbach, M. *J. Public Health* **1997**, *19*, 55−60.
(31) Feldman, J. M.; Kelley, W. N.; Lebovitz, H. E. *Diabetes* **1970**, *19*, 337−43.
(32) Rotblatt, M. D.; Koda-Kimble, M. A. *Diabetes Care* **1987**, *10*, 103−10.
(33) van der Sande, M. A. B.; Walraven, G. E. L.; Bailey, R.; Rowley, J. T. F.; Banya, W. A. S.; Nyan, O. A.; Faal, H.; Ceesay, S. M.; Milligan, P. J. M.; McAdam, K. P. W. J. *Trop. Med. Int. Health* **1999**, *4*, 506−513.
(34) Wei, O. Y.; Teece, S. *Emerg. Med. J.* **2006**, *23*, 139−140.
(35) Springsteen, G.; Wang, B. H. *Tetrahedron* **2002**, *58*, 5291−5300.
(36) Hisamitsu, I.; Kataoka, K.; Okano, T.; Sakurai, Y. *Pharm. Res.* **1997**, *14*, 289−293.
(37) Fritz, H.; Köhler, L.; Scherstén, B. *Assessment of Subnormal Urinary Glucose as an Indicator of Bacteriuria in Population Studies: An Investigation of 3,911 Subjects Between the Ages of Four and Sixty-five Years*, Series: Acta medica Scandinavica: Supplementum, Berling: Lund, 1969, Volume *504*, p 39.
(38) Wang, A.; Nizran, P.; Malone, M. A.; Riley, T. *Primary Care* **2013**, *40*, 687−706.
(39) Bensman, A.; Dunand, O.; Ulinski, T. Urinary Tract Infections. In *Pediatric Nephrology*; Avner, E., Harmon, W., Niaudet, P., Yoshikawa, N., Eds.; Springer: Berlin, 2009; pp 1297−1310.
(40) Talasniemi, J. P.; Pennanen, S.; Savolainen, H.; Niskanen, L.; Llesivuori, J. *Clin. Biochem.* **2008**, *41*, 1099−1103.
(41) Kawasaki, T.; Akanuma, H.; Yamanouchi, T. *Diabetes Care* **2002**, *25*, 353−7.
(42) Luceri, C.; Caderni, G.; Lodovici, M.; Spagnesi, M. T.; Monserrat, C.; Lancioni, L.; Dolara, P. *Cancer Epidemiol., Biomarkers Prev.* **1996**, *5*, 167−171.
(43) Johner, S. A.; Libuda, L.; Shi, L.; Retzlaff, A.; Joslowski, G.; Remer, T. *Eur. J. Clin. Nutr.* **2010**, *64*, 1365−70.
(44) Tasevska, N.; Runswick, S. A.; Welch, A. A.; McTaggart, A.; Bingham, S. A. *Eur. J. Clin. Nutr.* **2009**, *63*, 653−9.
(45) Yetisen, A. K.; Martinez-Hurtado, J. L.; Garcia-Melendrez, A.; da Cruz Vasconcellos, F.; Lowe, C. R. *Sens. Actuators, B* **2014**, *196*, 156−160.

dx.doi.org/10.1021/nl5012504 | *Nano Lett.* 2014, 14, 3587−3593